Journal of Materials Research and Technology 37 (2025) 2258–2270

Contents lists available at ScienceDirect

Journal of Materials Research and Technology

journal homepage: www.elsevier.com/locate/jmrt

Grain size effects on strain localization and fracture behavior in ferrite–martensite dual-phase steels characterized by digital image correlation analysis

Myeong-heom Park [a,*], Yuichi Tagusari [a], Akinobu Shibata [a,b], Nobuhiro Tsuji [a,c,**]

[a] Department of Materials Science and Engineering, Kyoto University, Yoshida Honmachi, Sakyo-ku, Kyoto, 606-8501, Japan
[b] Research Center for Structural Materials, National Institute for Materials Science (NIMS), 1-2-1 Sengen, Tsukuba, 305-0047, Japan
[c] Elements Strategy Initiative for Structural Materials (ESISM), Kyoto University, Yoshida Honmachi, Sakyo-ku, Kyoto, 606-8501, Japan

ARTICLE INFO

Handling editor: SN Monteiro

Keywords:
Dual phase steel
Mechanical properties
Digital image correlation (DIC)
Strain distribution
Micro void
Fracture

ABSTRACT

Dual-phase (DP) steels, consisting of soft ferrite and hard martensite phases, are widely utilized for their favorable balance of strength and ductility. Grain refinement in DP steels has been recognized as an effective strategy to enhance strength without sacrificing ductility, particularly in the post-uniform elongation regime. In the present study, the underlying mechanism responsible for improved post-uniform elongation through grain refinement was investigated using high-resolution digital image correlation (DIC) and detailed microstructural analysis of micro-void evolution. Two DP microstructures with ferrite grain sizes of 28.9 μm and 11.8 μm were fabricated, exhibiting markedly different local deformation behaviors. The fine-grained DP specimen (11.8 μm) exhibited more homogeneous deformation, attributed to a greater contribution of martensite to plastic deformation. Numerous micro-voids were observed in the fine-grained DP specimen, most of which remained small even under large deformation. In contrast, the coarse-grained specimen (28.9 μm) exhibited fewer micro-voids, several of which showed notable growth, potentially acting as fracture initiation sites, and contributing to limited post-uniform elongation. DIC analysis at the fracture stage successfully captured the strain distribution, revealing that micro-voids and cracks were predominantly located in regions with high strain gradients. These observations suggest that grain refinement may promote ductility by mitigating strain localization and reducing the propensity for void growth.

1. Introduction

A low-carbon dual phase (DP) steel, consisting of soft ferrite and hard martensite, is one of the most widely used practical steels for automotive sheet components due to its excellent balance of strength and ductility, as well as good formability at room temperature. The mechanical properties of DP steels vary widely depending on microstructural factors such as grain size, phase fraction, and hardness of each constituent phase [1–10]. Among these factors, grain refinement has been identified as the most effective strategy for simultaneously achieving high strength and large ductility [2,6–8]. To understand the origin of the exceptional mechanical performance enabled by grain refinement, it is essential to quantitatively investigate the local deformation behavior at the microstructural scale. However, the complex morphology of ferrite and martensite phases, including their irregularly shaped interfaces, poses a significant challenge in elucidating the underlying deformation mechanisms in DP structures.

Recently, digital image correlation (DIC), a technique capable of providing detailed local strain distribution, has emerged as a powerful tool for characterizing deformation heterogeneity [11–14]. Many research groups actively applied DIC to the study of DP steels [4,8–10,15–18]. These DIC-based studies have revealed that DP structures undergo highly heterogeneous deformation, often accompanied by pronounced strain localization in the soft ferrite phase [4,15]. Moreover, both the strain distribution and the intensity of strain localization have been shown to vary significantly depending on microstructural factors. Notably, recent findings indicate that grain refinement suppresses strain localization in soft ferrite, thereby enabling large ductility while

* Corresponding author.
** Corresponding author. Department of Materials Science and Engineering, Kyoto University, Yoshida Honmachi, Sakyo-ku, Kyoto, 606-8501, Japan.
E-mail addresses: park.myeongheom.8r@kyoto-u.ac.jp (M.-h. Park), nobuhiro-tsuji@mtl.kyoto-u.ac.jp (N. Tsuji).

https://doi.org/10.1016/j.jmrt.2025.06.165
Received 20 May 2025; Received in revised form 15 June 2025; Accepted 21 June 2025
Available online 23 June 2025

maintaining high strength [8,16–18]. However, to gain a deeper understanding of the mechanisms behind enhanced post-uniform elongation achieved through grain refinement, it is essential to investigate the deformation structure and its strain evolution under large plastic deformation, particularly in the vicinity of fracture.

Micro-void formation and growth are also critical factors to consider when discussing the deformation and fracture mechanisms in DP steels. Considering that the process of micro-void formation and growth becomes prominent after the onset of macroscopic necking [19–21], the enhancement of post-uniform elongation through grain refinement may be closely related to the suppression of micro-void evolution. Numerous studies have reported that micro-voids do not form randomly, but rather tend to be localized in two characteristic regions: at the ferrite/-martensite (F/M) boundary and within the martensite interior [3,22–25]. C.C. Tasan et al. [26] comprehensively summarized the influence of ferrite grain size and martensite volume fraction on micro-void formation sites, showing a clear trend: martensite cracking occurs predominantly in specimens with high martensite volume fractions, while ferrite-martensite decohesion is more frequently observed in specimens with larger ferrite grain sizes. Based on these prior findings, it is considered that the predominant sites of micro-void formation are strongly influenced by heterogeneous deformation behavior. Therefore, DIC-based strain analysis is expected to offer valuable insights, particularly in identifying the local strain conditions required for the initiation and growth of micro-voids.

In the present study, the origin of the improved stress-strain response achieved through grain refinement is investigated by characterizing local deformation behavior and micro-void evolution. This is accomplished through DIC-based strain analysis combined with detailed microstructural observations of deformed DP structures with different ferrite grain sizes.

2. Experimental procedure

A low-carbon steel with the chemical composition of Fe–2Mn-0.1C (wt.%) was used in the current study. The detailed thermo-mechanical processing route for obtaining dual-phase (DP) structures with different grain sizes is illustrated in Fig. 1. First, a homogenization heat treatment was performed at 1200 °C for 3 h under vacuum conditions. The homogenized specimens were then cold-rolled to a 90 % reduction in thickness. Subsequently, the cold-rolled specimens were subjected to heat treatment at two different austenitizing temperatures, 950 °C and 830 °C for 3 h, followed by furnace cooling to room temperature. This process resulted in ferrite + pearlite (F + P) microstructures with different ferrite grain sizes. Details of the grain size control and the corresponding microstructure evolution can be found in our previous studies [27,28]. The F + P specimens were then intercritically annealed at 750 °C for 1 h, followed by water-quenched to obtain ferrite + martensite DP structures with distinct ferrite grain sizes.

Microstructural observations were conducted using a field emission scanning electron microscope (FE-SEM; JEOL, JSM-7800F) operated at an accelerating voltage of 15 kV. Prior to SEM analysis, the specimens were mechanically polished using a series of emery papers ranging from #240 to #4000 grits, followed by electrolytic polishing in a solution consisting of 90 vol% of CH_3COOH and 10 vol % of $HClO_4$. Electrolytic polishing was performed at 22 V for 30 s at room temperature. Ferrite grain size was measured using the linear interception method, and the martensite volume fraction was estimated via the point-counting method based on the acquired SEM microstructure images.

The mechanical properties of the DP specimens were evaluated using a uniaxial tensile testing machine (Shimadzu, AG-100kN Xplus) at room temperature under quasi-static loading conditions with an initial strain rate of $8.3 \times 10^{-4}\ s^{-1}$. The tensile axis was aligned parallel to the rolling direction of the sheets. Tensile specimens were machined using an electrical discharge machine (Brother, HS-70A) and had a gauge length of 10 mm, a width of 2.5 mm, and a thickness of 0.5 mm.

Tensile strain and strain distribution were precisely measured using the digital image correlation (DIC) technique with a dedicated analysis software (Vic-2D, Correlation Solutions). Prior to tensile testing, the specimen surface was painted with black and white inks to produce a random speckle pattern for DIC strain analysis. During tensile testing, images of the speckle-patterned surface were captured at a constant frame rate of 5 fps using a CCD camera (SVS625MFCP, SVS-VISTEK). The acquired image sequences were processed for DIC analysis with a subset size of 0.11 mm × 0.11 mm and a strain measurement step of 0.017 mm.

In addition, microscopic DIC (μ-DIC) analysis was performed to characterize local deformation behavior at the microstructural scale. To generate an appropriate speckle pattern for μ-DIC analysis, the electrolytically polished specimen surface was coated with a colloidal silica suspension (SiO_2, average particle radius: 0.04 μm). The resulting surfaces used for μ-DIC are shown in Fig. 2. Tensile tests were interrupted at predetermined strain levels to observe the same area in SEM. For the μ-DIC analysis, the subset size and strain measurement step were set to 2.3 μm × 2.3 μm and 0.39 μm, respectively. High-resolution SEM images with a 2560 × 2048 pixel size were captured to examine detailed strain distribution and identify small micro-voids in regions approaching tensile fracture.

3. Results

3.1. Microstructural features of DP specimens with different grain sizes

Fig. 3 presents SEM micrographs of the DP specimens subjected to different heat treatments: (a) heating at 950 °C for 3h followed by furnace cooling (F.C.) and subsequent heating at 750 °C for 2h followed by water quenching (W.Q.); and (b) heating at 830 °C for 3h (F.C.) followed by 750 °C for 2h (W.Q). The microstructures were observed along the normal direction (ND) of the rolled sheet. In the SEM images, the letters **F** and **M** indicate ferrite and martensite phases, respectively.

The two DP specimens exhibited notably different ferrite grain sizes, while maintaining similar microstructural characteristics, including a

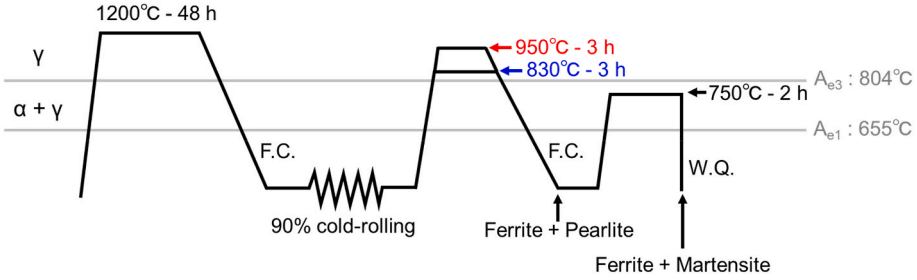

Fig. 1. Thermo-mechanical processing route for fabricating ferrite + martensite dual-phase (DP) microstructures with different ferrite grain sizes. The critical transformation temperatures, A_{e1} (655 °C) and A_{e3} (804 °C), were estimated using Thermo calc™ software with the TCFE7.0 thermodynamic database for steels and Fe-based alloys.

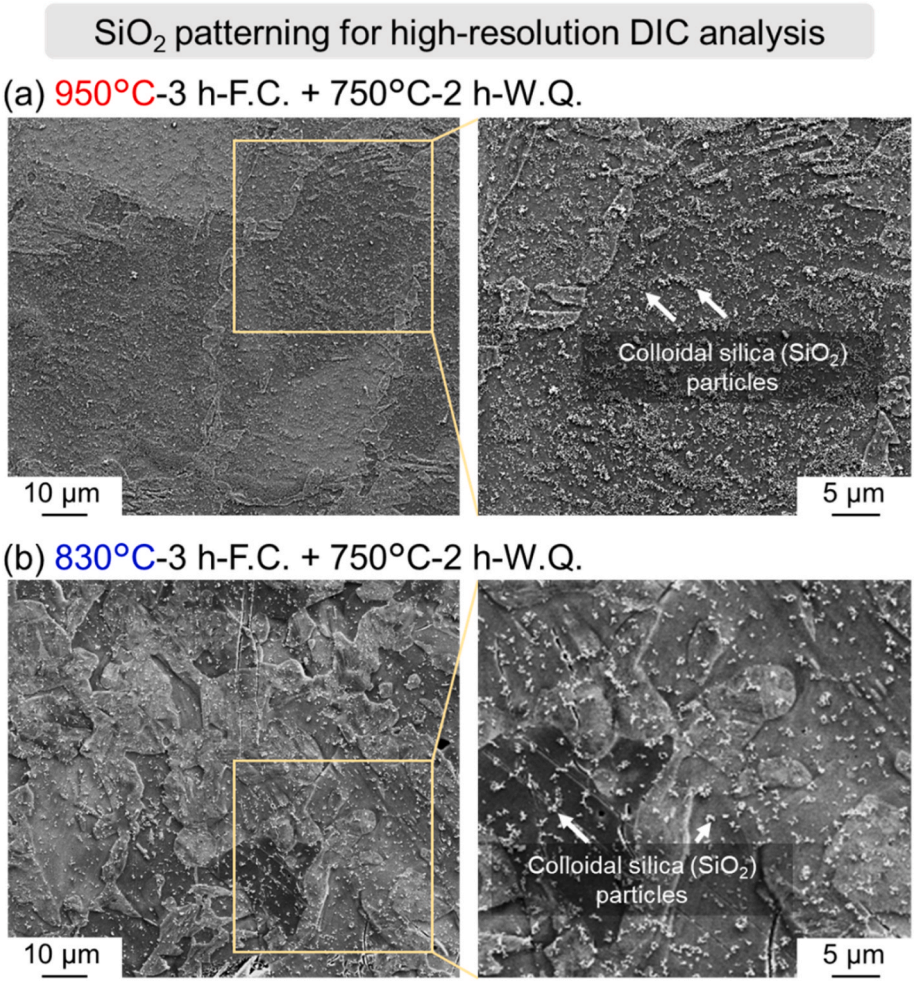

Fig. 2. SiO_2 patterning on electro-polished microstructures for high-resolution DIC analysis in specimens heat-treated at (a) 950°C-3 h-furnace cooling (F.C.), followed by 750°C-2 h-water quenching (W.Q.), and (b) 830°C-3 h-furnace cooling (F.C.), followed by 750°C-2 h-water quenching (W.Q.). Enlarged views of the yellow square regions are shown to the right of each original image. Colloidal silica (SiO_2) particles used for patterning are indicated by white arrows.

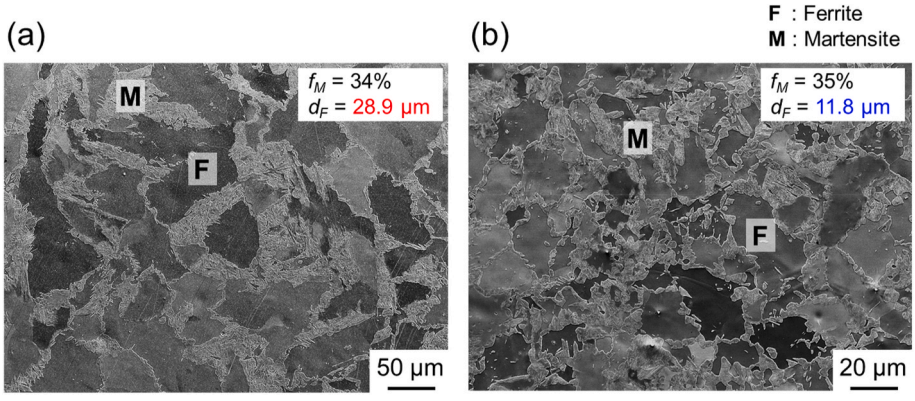

Fig. 3. SEM microstructures of DP specimens subjected to heat treatments of (a) 950 °C-3h-F.C. + 750 °C-2h-W.Q. and (b) 830 °C-3h-F.C. + 750 °C-2h-W.Q. Ferrite (F) and martensite (M) phases are labeled, with martensite volume fraction (f_M) and average ferrite grain size (d_F) indicated in each image.

martensite volume fraction of approximately 35 % and a phase distribution characterized by chain-like martensite surrounding the ferrite grains. The average ferrite grain sizes were 28.9 μm and 11.8 μm for specimens (a) and (b), respectively. These are hereafter referred to as "coarse-grained DP" and "fine-grained DP" specimens, respectively. While the primary focus of this study is on the effect of ferrite grain size, it should be noted that the martensite size also varies with changes in ferrite grain size. This aspect will be discussed in a later section.

3.2. Tensile properties

Fig. 4 (a) presents the nominal stress-strain (S–S) curves of the coarse-grained DP (red) and fine-grained DP (blue) specimens. A circle symbol on each curve indicates the point of uniform elongation. The

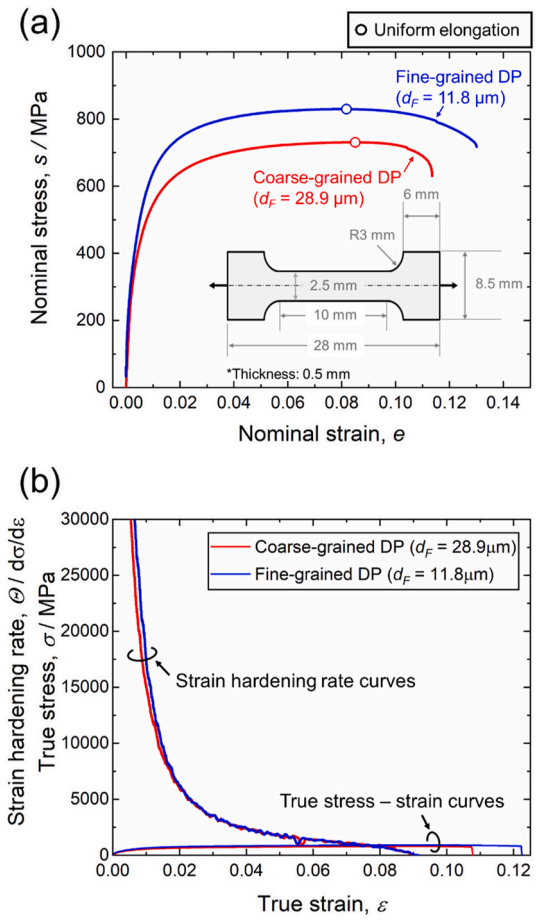

Fig. 4. (a) Nominal stress-strain curves and (b) strain hardening rate curves with true stress-strain curves for the coarse-grained DP specimen (28.9 μm, red)) and fine-grained DP specimen (11.8 μm, blue). The uniform elongation point is indicated by a circle on each nominal stress-strain curve. A schematic illustration of the tensile specimen is inserted in (a) for reference.

fine-grained DP specimen (11.8 μm) achieved a superior combination of strength and ductility, exhibiting a high ultimate tensile strength (UTS) of 830 MPa and a large total elongation of 13.0 %, compared to the coarse-grained DP specimen (28.9 μm) with a UTS of 731 MPa and a total elongation of 11.4 %. Although the two specimens exhibited similar uniform elongations (8.6 % for coarse-grained DP and 8.2 % for fine-grained DP), the fine-grained DP specimen demonstrated a more pronounced post-uniform elongation (4.9 %) compared to the coarse-grained DP specimen (2.9 %). According to Considère criterion [29], the uniform elongation can be interpreted based on the onset of macroscopic plastic instability, which occurs when the strain-hardening rate curve intersects the true stress-strain curve.

Fig. 4 (b) displays the strain hardening rate curves of the coarse-grained DP and fine-grained DP specimens, along with their corresponding true stress-true strain curves. Both specimens exhibited the typical strain hardening behavior observed in metallic materials, characterized by a monotonic decrease in the strain hardening rate with increasing plastic deformation. The fine-grained DP specimen showed a slightly higher strain hardening rate than the coarse-grained DP specimen up to a true strain of approximately 0.02, after which both specimens exhibited nearly identical strain hardening rates. Consequently, the uniform elongation, determined by the intersection of the strain hardening rate curve with the true stress-strain curve according to the Considère criterion, occurred at a relatively large true strain for the fine-grained DP specimen, contributing to its enhanced uniform elongation.

3.3. Local deformation behavior by DIC strain analysis

To further investigate the deformation behavior at the microscale, local strain distributions during tensile deformation were characterized. Fig. 5 shows SEM deformation microstructures and corresponding μ-DIC strain distribution maps, along with local strain profiles, for (a) coarse-grained DP and (b) fine-grained DP specimens tensile-deformed to ~5.5 %. The tensile direction is parallel to the horizontal direction of the images.

In the μ-DIC maps, the colors superimposed on the SEM images represent the normal strain in the tensile direction (ε_{11}), according to the key color bar provided. In the SEM images, numerous slip lines were observed mostly within the ferrite grains of both DP specimens, indicating that the softer ferrite phase experienced more pronounced plastic deformation. It should be noted that the DIC analysis employed here is based on a two-dimensional approach, which does not account for surface roughness or out-of-plane strain components. Such limitations may affect strain estimation accuracy, particularly under conditions involving significant surface topography. This issue may be addressed in future studies by integrating thickness-profile measurement techniques to enhance strain field reconstruction. Despite these limitations, the present study evaluates local deformation based on the normal strain component in the tensile direction (ε_{11}). In the corresponding DIC strain color map, the two DP specimens exhibited distinctly different strain distributions, despite having nearly the same average strain value (ε_{11}) in the DIC-analyzed regions (0.060 for the coarse-grained DP specimen and 0.059 for the fine-grained DP specimen).

Strong strain localization was observed in the coarse-grained DP specimen, characterized by the development of several strain-localized bands with strain values exceeding 0.15 (red color), while the surrounding regions outside these bands exhibited extremely low strain values close to zero (purple color). In contrast, the fine-grained DP specimen exhibited relatively homogeneous deformation without pronounced strain localization. Instead, numerous weak strain-localized bands with strain values ranging from 0.07 to 0.11 (green color range) were predominantly observed. The regions outside the strain-localized bands also contributed slightly to plastic deformation, as indicated by light purple or blue areas in the fine-grained DP specimen. To clarify the strain distribution, strain line analysis was performed along a horizontal inspection line passing through the center of the DIC strain map. Severe strain fluctuations with a periodic pattern were observed in both DP specimens. The locations of strain peaks were number-tagged in the strain profiles, revealing 7 peaks in the coarse-grained DP specimen and 12 peaks in the fine-grained DP specimen. The average strain along the inspection line was 0.0576 for the coarse-grained DP and 0.0607 for the fine-grained DP specimens. However, the degree of strain localization differed notably, as indicated by the average peak strain value of 0.113 ± 0.0502 for the coarse-grained DP specimen (based on 7 strain peaks) and 0.084 ± 0.0219 for the fine-grained DP specimen (based on 12 strain peaks). These results suggest that the coarse-grained DP specimen exhibited more severe strain fluctuations, indicating a more heterogeneous deformation behavior. Peak intervals—defined as the top-to-top distance between adjacent peaks—also differed between the two DP specimens. The average peak interval on the lines was 49.0 ± 21.3 μm for the coarse-grained DP specimen and 27.7 ± 28.6 μm for the fine-grained DP specimen. Given that strain localization predominantly occurs in the ferrite phase, these peak intervals likely reflect both the distribution and size of ferrite grains.

To further examine the relationship between phase distribution and strain localization, a detailed analysis was conducted. Fig. 6 presents phase distribution sketches and DIC strain distribution maps for (a) the coarse-grained DP specimen and (b) the fine-grained DP specimen at different strain levels. In the sketches, light blue and dark blue colors indicate ferrite (**F**) and martensite (**M**), respectively, and the tensile direction is aligned with the horizontal axis of the images. Colors in the DIC strain map represent the normal strain (ε_{11}) along the tensile axis. In

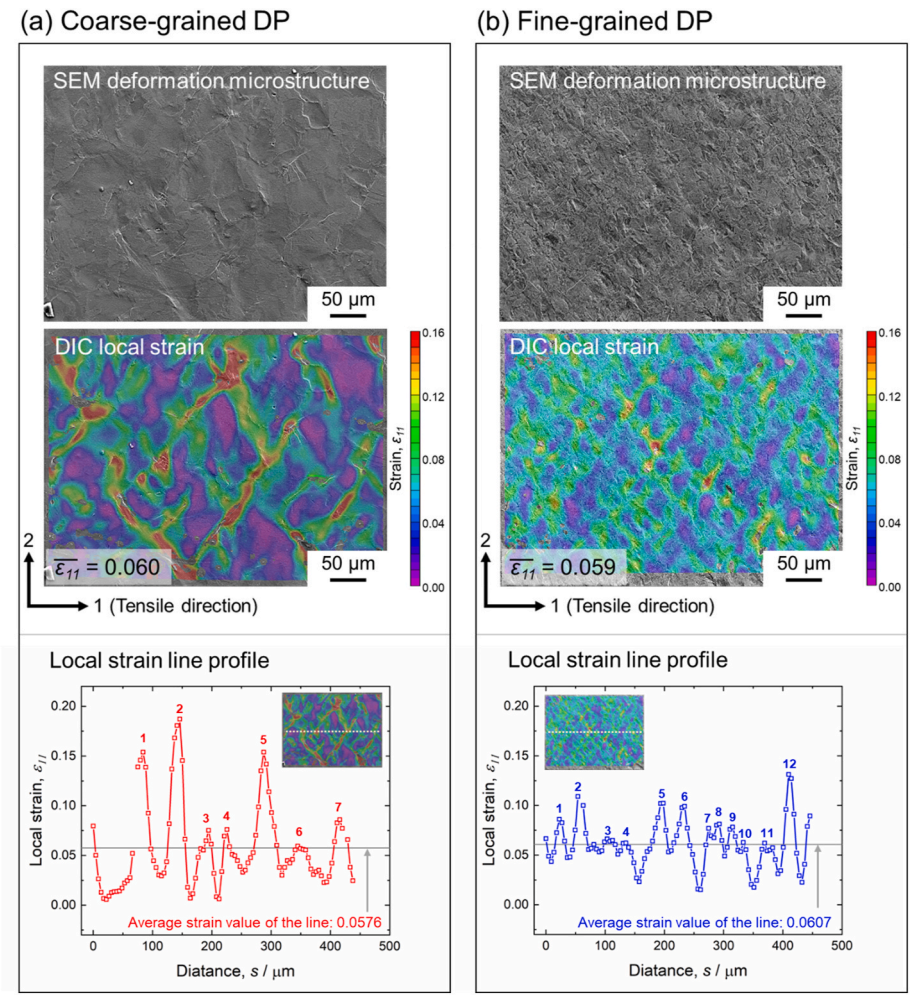

Fig. 5. SEM deformation microstructures and corresponding DIC strain distribution maps with local strain line profiles for (a) the coarse-grained DP and (b) the fine-grained DP specimens. The color overlays on the DIC maps represent the normal strain component in the tensile axis (ε_{11}), as referenced by the color scale bar. Strain line profiles were extracted along the horizontal line passing through the center of each DIC strain map.

the coarse-grained DP specimen, strain-localized bands were found to develop preferentially along ferrite/martensite (F/M) interfaces. These bands propagated selectively through regions containing thin martensite with small volume fractions, suggesting that such small volume-fractioned thin martensite does not serve as effective barriers to hinder strain propagation. In contrast, as indicated by the white arrows in Fig. 6 (a), thick, equiaxed martensite regions with larger volumes remained nearly undeformed in the coarse-grained DP specimen, exhibiting near-zero strain values (purple color; $\varepsilon_{11} \sim 0$) even at relatively high average strain levels ($\varepsilon_{11}^{average} = 0.058$). A similar tendency—where strain localization primarily occurred within ferrite grains—was also observed in the fine-grained DP specimen; however, the magnitude of localized strain was comparatively lower. In addition, the propagation of strain-localized bands in the fine-grained DP specimen was frequently interrupted by martensite regions, as highlighted by the white arrows in Fig. 6 (b). In terms of propagation linearity, the strain-localized bands in the fine-grained DP specimen tended to follow more linear paths, whereas those in the coarse-grained DP specimen showed curved propagation, likely due to the effective blocking by large martensite particles. These observations indicate that martensite size plays a significant role, particularly in disrupting the continuity of strain-localized bands, while the overall strain distribution is predominantly governed by ferrite grain size. The pronounced difference in local strain distribution behavior between the two DP specimens is considered to significantly influence the evolution of micro-void formation/growth, as strain-localized regions and their vicinity are known to serve as preferential sites for micro-void initiation [30–32].

3.4. Quantitative observation of micro-void evolution

Fig. 7 shows DIC strain maps and corresponding deformation microstructures for (a) the coarse-grained DP and (b) the fine-grained DP specimens. Four rectangular regions (Areas 1 to 4) in each SEM micrograph highlighted representative zones experiencing strain localization, with their magnified views indicated on the right. Micro-voids identified through SEM observations are indicated by black arrows in the enlarged images. In the coarse-grained DP specimen, micro-voids were distinctly observed in the vicinity of strain-localized regions. These voids appeared to form either at ferrite/martensite (F/M) boundaries (Areas 1 and 4 in Fig. 7 (a)) or within the martensite phase itself (Area 2 in Fig. 7 (a)). No distinct micro-voids were observed in Area 3 in Fig. 7 (a). In the fine-grained DP specimen, micro-voids were also found within strain-localized regions (Area 2 in Fig. 7 (b)). However, the clear identification of micro-voids was more challenging due to pronounced surface roughening in the fine-grained DP specimen, suggesting that careful surface preparation—such as polishing in the plastically deformed state after UTS—is essential to enable more accurate observation of micro-void evolution.

Fig. 8 presents SEM images of the deformation microstructure and corresponding micro-void distribution maps for (a) coarse-grained DP

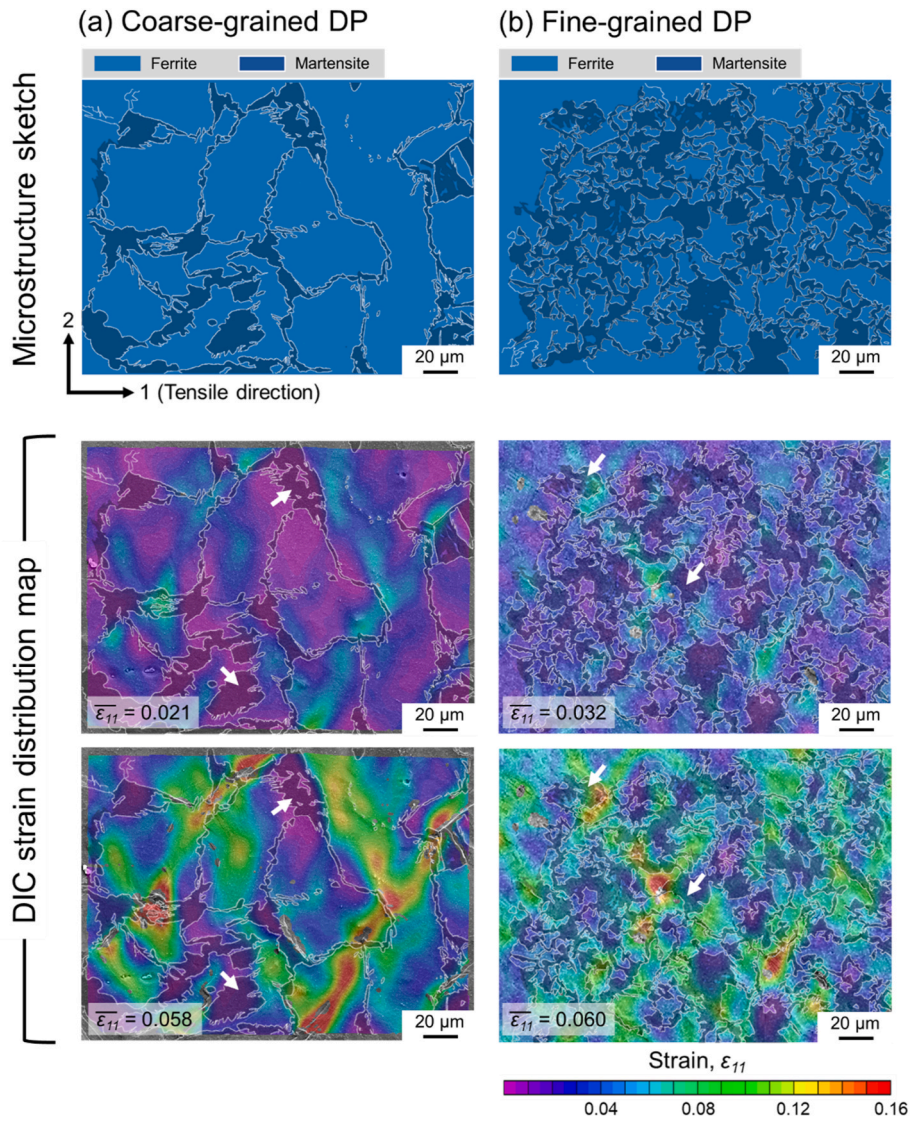

Fig. 6. Microstructure sketches and DIC strain distribution maps of (a) the coarse-grained DP specimen and (b) the fine-grained DP specimen under different deformation conditions. In the sketches, light blue and dark blue indicate ferrite and martensite, respectively. The colors in the DIC map correspond to the normal strain component along the tensile axis (ε_{11}). Arrows indicate the locations of large-sized martensite.

and (b) fine-grained DP specimens in the post-uniform elongation regime, approaching tensile fracture. To clearly reveal the distribution of micro-voids, the coarse-grained DP specimen was pre-polished at a tensile strain of 7.5 %, and the fine-grained DP specimen was pre-polished at 9.7 %. Micro-void evolution was examined at strains of 10.2 % and 10.9 % (just before fracture) for the coarse-grained DP specimen, and at 11.6 % and 12.2 % (just before fracture) for the fine-grained DP specimen. The tensile loading is parallel to the horizontal axis of images, and the main crack path is indicated by a solid line, traced along the tensile fracture surface. Micro-voids are shown as black features in micro-void distribution maps. A considerable number of micro-voids were observed in both DP specimens, and some exhibited a notable growth with further deformation. However, a clear difference in both the number and size of voids was observed between the two specimens. In the coarse-grained DP specimen, the number of voids (n_{void}) was 32 at a tensile strain of 10.2 %, increasing to 42 at 10.9 %, indicating the formation of only 10 additional micro-voids. In contrast, the fine-grained DP specimen exhibited 31 micro-voids at a strain of 11.6 %, which dramatically increased to 74 at 12.2 %, suggesting a significantly more active void nucleation process.

Void size was evaluated based on void-occupied area [μm^2]. In the coarse-grained DP specimen, the total void-occupied area increased significantly from 101 μm^2 (area fraction, f^{Area}: 6.65×10^{-4}) to 288 μm^2 (f^{Area}: 18.98×10^{-4}) as the tensile strain increased. In contrast, the fine-grained DP specimen showed a smaller increase, from 60 μm^2 (f^{Area}: 3.95×10^{-4}) to 106 μm^2 (f^{Area}: 6.65×10^{-4}). Notably, large micro-voids with lengths exceeding 30 μm were more frequently observed in the coarse-grained DP specimen at the tensile strain of 10.9 %. These results suggest that while the fine-grained DP specimen contains a large number of micro-voids, most of them remain small in size without undergoing significant growth. On the other hand, only a few micro-voids were observed in the vicinity of the main crack. In other words, no significant concentration of micro-voids was detected in the region where the main crack occurred. This is likely because the crack initiation site was located outside the observed area, and the main crack passed incidentally through the observed region. Nevertheless, it is worth noting that the incidentally passing main crack exhibits a zig-zag morphology in both specimens, suggesting that even during its abrupt propagation, the crack path is influenced by microstructural features and/or local deformation behaviors. This aspect will be further explored in the discussion section.

The void formation sites, along with the corresponding void number

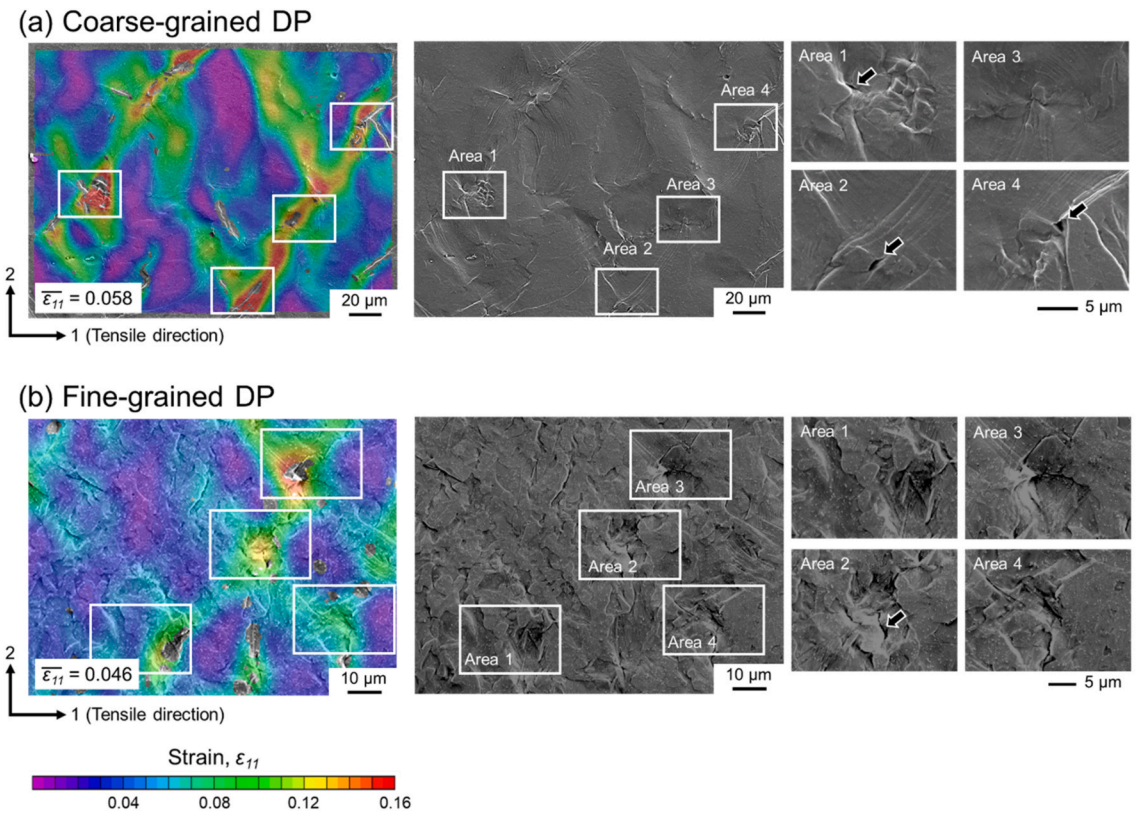

Fig. 7. DIC strain maps and corresponding SEM deformation microstructures of (a) the coarse-grained DP specimen and (b) the fine-grained DP specimen. Four boxed regions (Area 1 to Area 4) on each SEM image indicate representative zones of strain localization, with enlarged views shown on the right. Black arrows in the SEM images indicate the presence of micro-voids.

and sizes, are summarized in Table 1. Based on the data in Fig. 8 and Table 1, quantitative analyses are shown in Fig. 9, including: (a) the total number, (b) the total size of observed micro-voids, and (c) the number of micro-voids classified by their formation sites—ferrite, martensite interiors and ferrite/martensite (F/M) boundaries—at different deformation stages for both coarse-grained and fine-grained DP specimens. In Fig. 9 (a) and Fig. 9 (b), the polishing point for each specimen is indicated by a black arrow, at which the void number and size are assumed to be zero. As briefly discussed in Fig. 8, the coarse-grained DP specimen exhibited lower total number but higher total sizes of micro-voids compared to the fine-grained DP specimen. Furthermore, Fig. 9 (c) revealed that micro-voids were primarily formed within the martensite interior and at ferrite/martensite (F/M) boundaries. This trend is consistent with findings reported in previous studies by other research groups [22,24–26]. The ferrite interior was not a predominant site for void formation in either DP specimen. Overall, micro-voids were more frequently initiated within the martensite interior than at the ferrite/martensite (F/M) boundaries. Interestingly, however, the fine-grained DP specimen exhibited a notable increase in void formation by F/M boundary decohesion, suggesting a shift in the dominant void nucleation mechanism under refined grain conditions.

4. Discussion

4.1. In-situ observation of fractured regions using digital image correlation techniques

As mentioned in the result section, the observed region does not necessarily correspond to the initial crack nucleation site, but rather to an area through which the main crack propagated. Despite the incidental and rapid nature of fracture, the zig-zag morphology of the crack path suggests a significant influence from local strain fields and/or the spatial distribution of microstructural phases. To explore this relationship, DIC strain analysis was coupled with microstructural observations.

Table 1
Summary of micro-void characterization involving formation site, void count, and total void area.

Specimen	Grain size of ferrite	Strain	Micro-void characterization in number and size					
			Micro-void number in specific formation sites				Total micro-void area (size) in observed area	
			Ferrite/martensite boundary	Martensite interior	Ferrite interior	Total	Total Area of micro-voids	Total Area fraction of micro-voids
Coarse-grained DP	28.9 μm	$e = 10.2$ %	6	26	0	32	101 μm^2	6.65×10^{-4}
		$e = 10.9$ %	8	33	1	42	288 μm^2	18.98×10^{-4}
Fine-grained DP	11.8 μm	$e = 11.6$ %	7	23	1	31	60 μm^2	3.95×10^{-4}
		$e = 12.2$ %	25	44	5	74	106 μm^2	6.98×10^{-4}

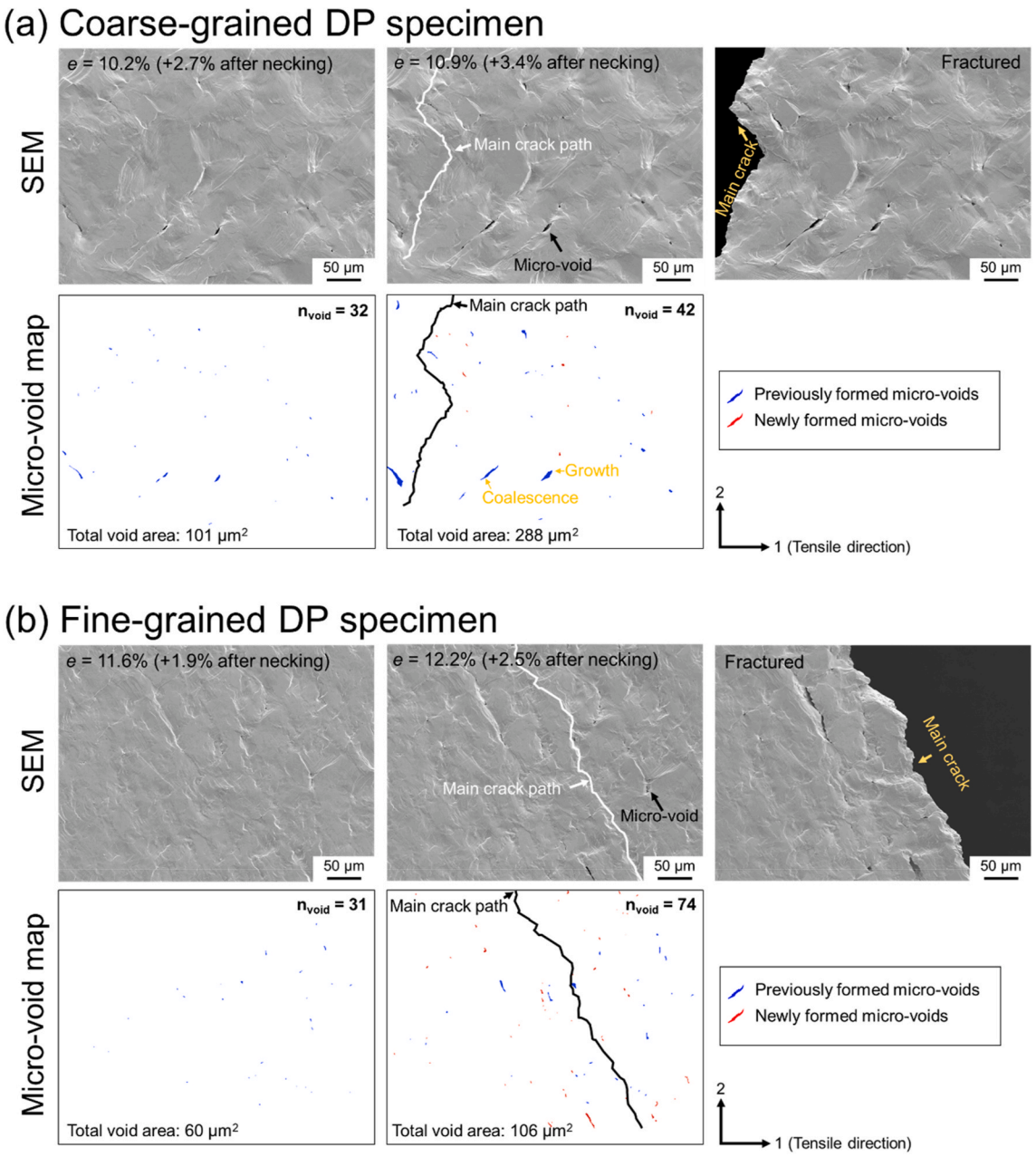

Fig. 8. SEM deformation microstructures and corresponding micro-void distribution maps of (a) coarse-grained DP and (b) fine-grained DP specimens in the post-uniform elongation stage to tensile fracture. The main crack path, corresponding to the fracture surface, is marked by a solid line. Previously formed and newly formed micro-voids are indicated in blue and red, respectively. The number of micro-voids (n_{void}) and total void-occupied area (void size, in μm^2) are provided in each micro-void distribution map.

Although predicting the exact site of crack propagation during DIC analysis is experimentally challenging due to the inherently stochastic nature of fracture, the present study successfully captured a cracking event through careful in-situ observation. Fig. 10 shows in-situ tracking of local strain evolution using DIC in the fracture region of (a) fine-grained and (b) coarse-grained DP specimens. The white solid lines indicate the traced fracture paths for each specimen. In the case of the fine-grained DP specimen, both a low-magnification microstructure image and the corresponding strain map are shown, along with enlarged views of Area 1. Micro-voids identified after fracture are marked by yellow arrows. DIC strain analysis was performed within the strain ranges of 11.6 %–12.2 % for the fine-grained DP specimen and 9.8 %–10.9 % for the coarse-grained DP specimen. In the low-magnification result of the fine-grained DP specimen, a significant surface roughness band was observed in the SEM image, corresponding to a macroscopic strain-localized band with an approximate width of 500 μm. As expected, this region experienced strong strain localization, indicating that crack initiation predominantly occurred within zones of localized plastic deformation. However, the observed zig-zag propagation path of the crack may be attributed to microstructural heterogeneity, particularly the irregular morphology and spatial distribution of martensite particles. Although the enlarged strain maps provided more detailed information on localized deformation, no significant strain localization was observed in the immediate vicinity of the main crack path. In the coarse-grained DP specimen, more heterogeneous deformation behavior was recognized. Nevertheless, a similarly weak relationship was found between the main crack path and areas of strain localization. On the other hand, several observed micro-voids were located in regions exhibiting

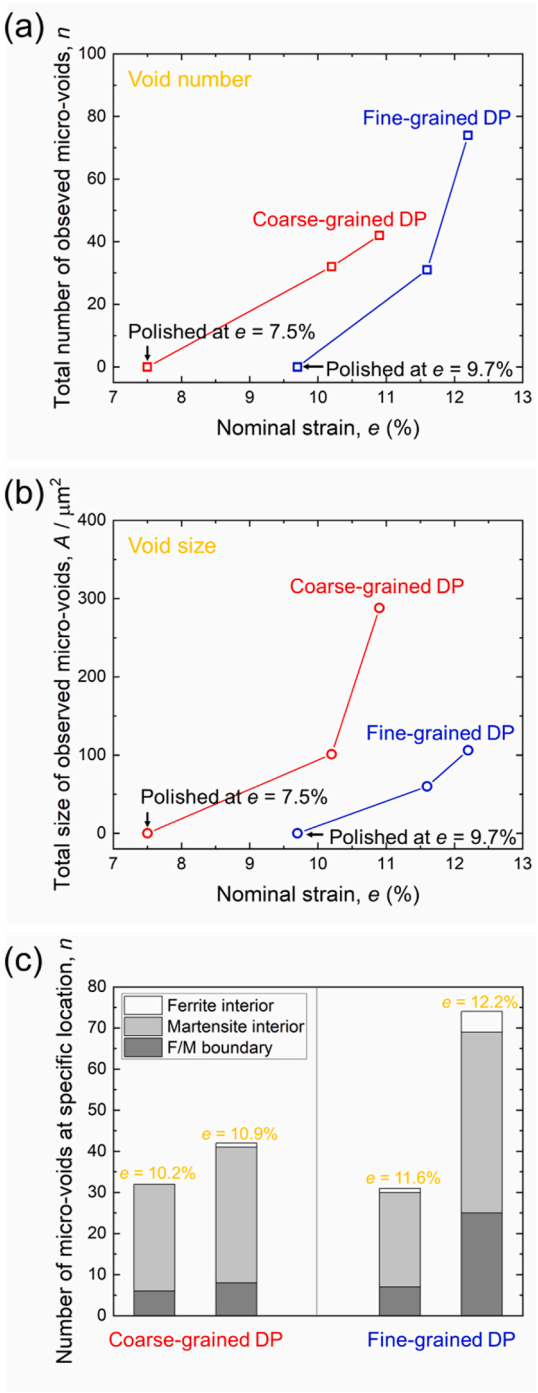

Fig. 9. Quantitative analysis in micro-void number and size. (a) Total number and (b) total size of micro-voids for the coarse-grained and fine-grained DP specimen. The polishing point for each specimen is indicated by a black arrow, where the void number and size are assumed to be zero. (c) Number of micro-voids separately identified in ferrite, martensite interiors and ferrite/martensite (F/M) boundaries at different deformation stages. All data are extracted from the micro-void distribution results shown in Fig. 8.

strain gradients, implying a potential link between local strain inhomogeneity and void formation. To further clarify the preferential sites of crack propagation and micro-void formation, a combined analysis of microstructural features and DIC-based strain evolution was performed.

Fig. 11 exhibits the results of identical-area SEM observation and DIC analysis, including strain distribution maps and the corresponding line profile. It should be noted that the tensile-fractured surface exhibited substantial surface roughness, which caused the loss of key microstructural features—such as the distribution of ferrite, martensite and their interfaces—even after pre-polishing. Therefore, the microstructural details were retrospectively reconstructed by referencing the microstructure observed in the pre-polished state. The ferrite/martensite (F/M) boundaries were marked with white lines, based on which the microstructure sketch was constructed. DIC strain distribution data on the same area were also provided. Red and pink circle symbols indicate the traced positions of the main crack and micro-voids, respectively, as identified with reference to the pre-polished SEM microstructure. These traced positions, determined through careful SEM observation, along with their connecting lines provide the approximate final locations of crack formation at tensile fracture. The positions of these circle symbols are also shown on the DIC strain distribution maps for reference, where the color scale represents the normal strain component (ε_{11}) in the tensile direction.

It was obvious that the main crack in the coarse-grained DP specimen propagated by detouring around bulky martensite and penetrating through thin martensite regions. The fine-grained DP specimens exhibited a similar propagation tendency; however, the crack frequently propagated across relatively large martensite islands. Overall, the zig-zag morphology of the main crack appears to result from the detouring process around large martensite regions during crack propagation. A similar trend was observed in the growth behavior of micro-voids. An interesting observation is that micro-void growth was halted at the ferrite/martensite (F/M) boundary. This suggests that micro-voids may propagate in a discontinuous manner, with growth temporarily arrested at each F/M interface—in other words, the F/M interface acts as an obstacle against micro-void growth. Such behavior provides experimental support for several previously proposed models or interpretations of crack propagation mechanisms [15,19,21]. The presence of large ferrite grains in the coarse-grained DP specimen may allow long-range void growth, as fewer obstacles exist within a single ferrite grain, which could partly explain the frequent formation of large-sized micro-voids. These findings highlight the importance of both ferrite and martensite size effects: coarse ferrite grains allow for longer propagation paths, while coarse martensite particles promote crack detouring during propagation.

Additionally, the DIC strain distribution results offer further insights into the evolution of the main crack and micro-voids. It was found from DIC strain maps and corresponding line profiles that both the main crack and micro-voids were not located in the regions with the highest strain localization, but rather along regions with significant strain gradient. This tendency was particularly pronounced in the coarse-grained DP specimen.

Since the strain gradient primarily develops along the F/M boundaries, as shown in Figs. 5 and 6, this phenomenon can be discussed in relation to strain compatibility at these interfaces. We suggest that the failure of strain compatibility at the F/M boundaries occurs due to the limited deformability of martensite and/or the excessive strain localization in ferrite. In this context, the distinct differences observed in the strain profiles (Fig. 6) between coarse- and fine-grained DP specimens may account for the variations in micro-void size and number. The coarse-grained DP specimen exhibited large strain gradients, although such sites were relatively few. In contrast, the fine-grained DP specimen showed numerous strain gradient sites, but each exhibited a comparatively lower strain gradient. It is reasonable to infer that the magnitude of strain gradients governs the ease of micro-void formation, whereas the number of gradient sites correlates with the total number of micro-voids. Accordingly, the fine-grained DP specimen tends to develop a greater number of micro-voids, but with smaller sizes. Furthermore, with respect to ductility, the number of micro-voids appears to be less critical than their size and growth. This can be one possible reason for exhibiting large post-uniform elongation of the fine-grained DP specimen.

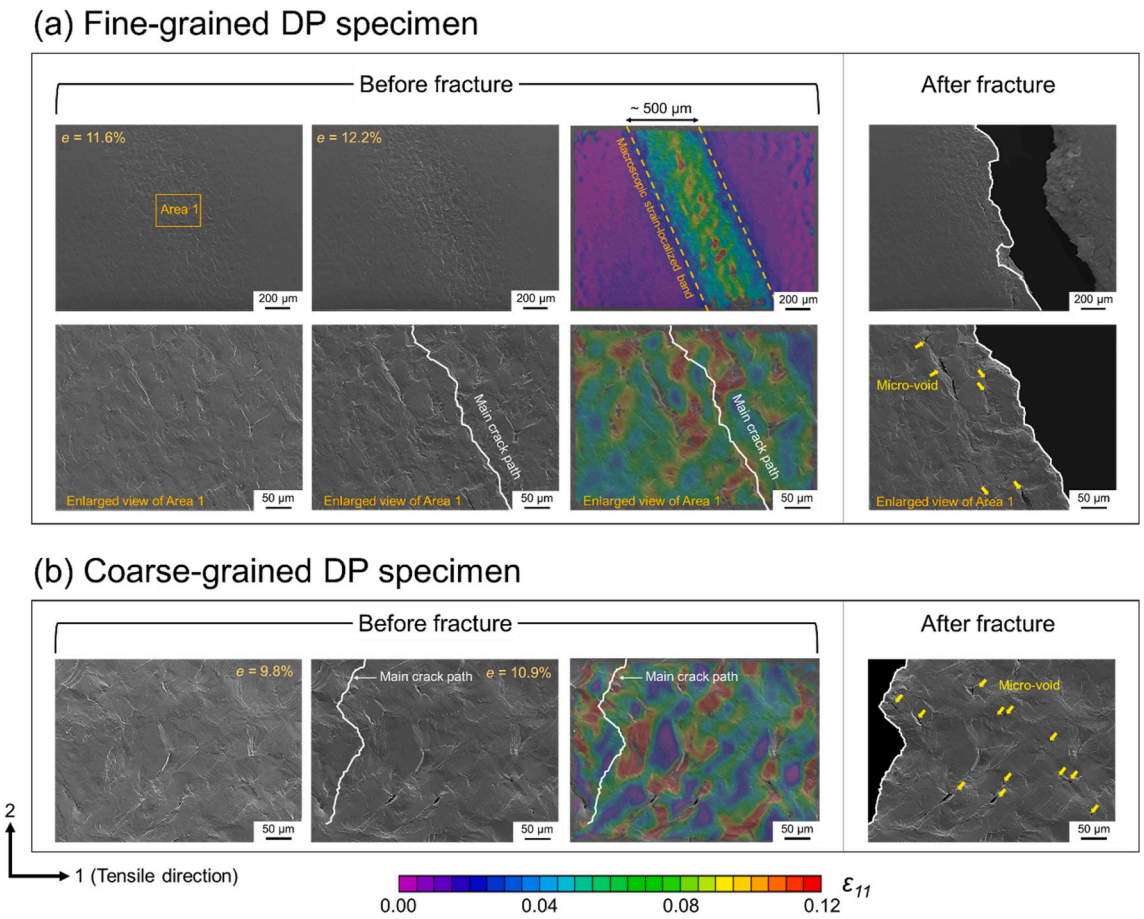

Fig. 10. In-situ tracking of local strain evolution using DIC in the fracture region of (a) fine-grained and (b) coarse-grained DP specimens. The white solid lines indicate the traced fracture paths for each specimen. For the fine-grained DP specimen, both a low-magnification microstructure image and the corresponding strain map are provided, along with enlarged views of Area 1. Micro-voids identified after fracture are marked by yellow arrows.

4.2. Effect of martensite size on the propagation of the main crack and micro-voids

As briefly discussed above, the main crack tends to preferentially propagate through thin martensite regions. In this section, we quantitatively evaluate the propagation lengths of the main crack and micro-voids, distinguishing between their progression within ferrite and martensite phases. Fig. 12 displays the results of a line fraction analysis performed along the paths of the main crack and micro-voids to evaluate phase-specific propagation. Fig. 12 (a) illustrates a representative example of the characterization method, while Fig. 12 (b) summarizes the results in the form of a bar graph, derived from the analysis of Fig. 11. In this analysis, ferrite and martensite phases are indicated in blue and pink, respectively, and crack/micro-void propagation is assumed to occur in the vertical (top-to-bottom) direction. In the coarse- and fine-grained DP specimens, the ferrite/martensite line fractions were 83 %/17 % and 71 %/29 %, respectively. In both specimens, the martensite fraction along the main crack path (17 % for coarse-grained and 29 % for fine-grained DP specimens) was significantly lower than the overall average martensite volume fraction (~35 %). This observation provides indirect evidence of a preferential crack propagation path that consistently traverses thin martensite regions with relatively low volume, as observed in Fig. 11. This tendency is more pronounced in the coarse-grained DP specimen, likely due to the presence of bulky martensite regions with large volume, which the crack tends to bypass. On the other hand, notably, in both specimens, nearly all martensite regions penetrated by cracks or voids were less than 10 μm in length. This suggests that the martensite acts as an effective barrier to crack or void propagation only when its size exceeds approximately 10 μm. More importantly, no significant difference in martensite length was observed between the main crack and adjacent micro-voids, implying that both features follow the same cracking mechanism. This finding highlights the importance of analyzing micro-voids to gain deeper insight into the fracture process, as they may serve as precursors to final fracture. While the present study primarily focused on crack and void propagation in relation to martensite size, the morphological characteristics of martensite may also play a critical role in micro-void initiation and growth. Azuma et al. [3,33] reported that narrow-shaped martensite segments tend to be preferential sites for cracking due to stress concentration arising from complex stress states—a phenomenon further supported by several simulation studies [21,34–36].

Based on the comprehensive experimental results, the limited post-uniform elongation observed in the coarse-grained DP specimen can be interpreted considering the following factors: (i) The presence of an extreme bimodal distribution in martensite grain size promotes strain localization. Large martensite regions act as strong barriers to strain propagation, leading to intense strain localization in adjacent ferrite grains. Conversely, small martensite segments, which do not function effectively as barriers, may facilitate the growth of voids. (ii) The large ferrite grains may also contribute to accelerated void growth, as micro-voids tend to propagate in a stepwise manner, propagating to ferrite grains and halting temporarily at each ferrite/martensite (F/M) boundary.

Although the difference in strain distributions associated with grain size variation is clear, the relationship with post-uniform elongation and micro-void evolution remains to be further elucidated due to the limited

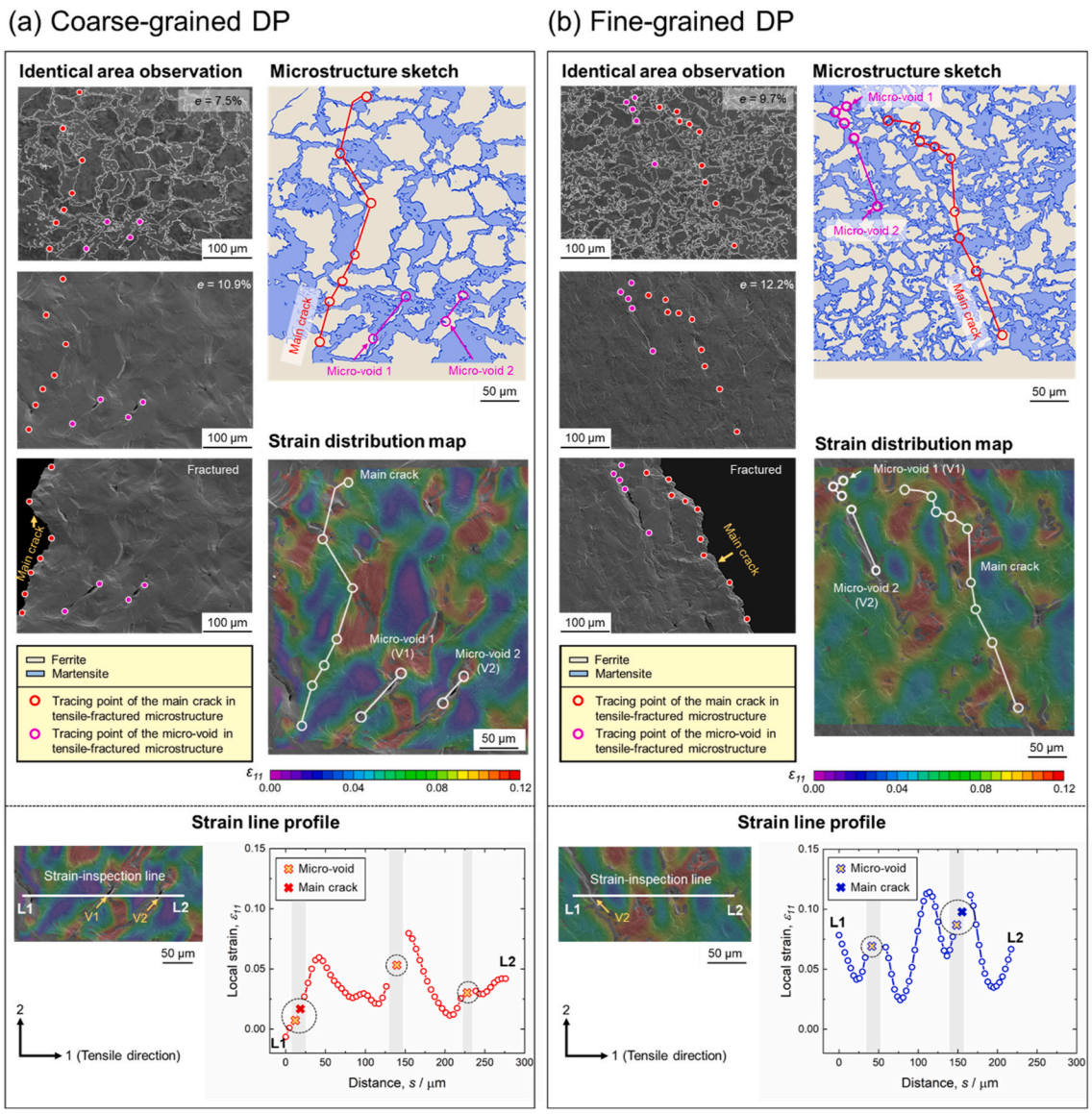

Fig. 11. SEM observations of identical areas and corresponding DIC strain distribution maps with strain line profiles for (a) the coarse-grained DP and (b) the fine-grained DP specimens at the later deformation stage near the tensile fracture. In the SEM images, the white solid line indicates the ferrite/martensite (F/M) boundary. Red and pink circles mark the traced positions of the main crack and micro-voids, respectively, as observed in the post-fracture microstructures. The color scale in the DIC maps represents the normal strain in the tensile axis (ε_{11}). Strain line profiles were extracted along inspection lines that pass through 2–3 micro-voids and the main crack location.

number of observations. This will be addressed in our future research. Moreover, it should also be emphasized that the observed differences in strain distribution and fracture behavior are not governed solely by grain size. Micro-void evolution and final fracture are inherently local phenomena, influenced by additional factors such as stress triaxiality [37] and various interfacial characteristics, which may give rise to complex local stress conditions. Although a direct linkage has not yet been fully established, the refinement of both ferrite and martensite appears to provide favorable conditions for reducing strain localization and void coalescence.

To further advance our understanding of the micro-void growth process in relation to grain size variation, more detailed microstructural investigations are necessary. In particular, the use of in-situ observation techniques for tracking micro-void evolution, combined with stress measurement approaches such as the EBSD-Wilkinson method [38,39], is expected to provide valuable insights and will be the focus of future work. In addition, numerical analysis using finite element method (FEM) simulations may serve as a complementary approach for identifying dominant sites of stress and strain localization [40]. Furthermore, in parallel, the adoption of higher-resolution DIC techniques employing gold nanoparticles as speckle markers [41,42] could offer deeper insight into the mechanisms of micro-void evolution at finer spatial scales. This approach will also be explored in subsequent studies.

While the present study primarily examined the influence of ferrite and martensite sizes on local strain distribution and crack propagation behavior, it is important to acknowledge that the deformation response of dual-phase (DP) structures may also be affected by additional factors. These include the strength (or hardness) contrast between the constituent phases [10], the specific morphology of martensite particles [4,9,43], and phase fractions [44], which were not explicitly addressed in this work. Nevertheless, the present findings provide important guidance for the microstructural design of dual-phase (DP) steels, suggesting that refining both ferrite and martensite sizes is an effective strategy to simultaneously enhance strength and ductility by mitigating strain localization and suppressing micro-void growth.

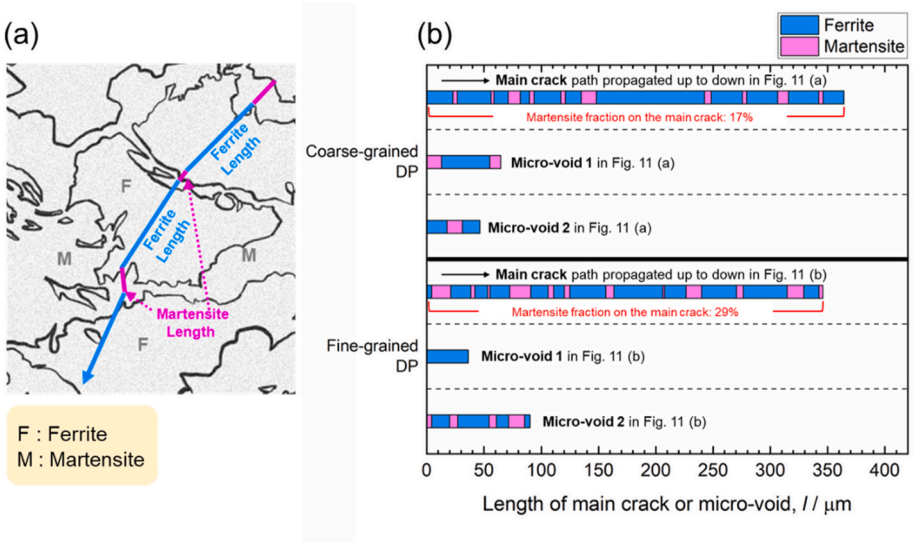

Fig. 12. Quantitative analysis of crack and micro-void propagations based on the line fraction of ferrite and martensite phases along the crack path. (a) Example illustrating the method used to measure the line fraction of each phase along the propagation line. (b) Bar graph showing the line fraction of ferrite (blue) and martensite (pink) along the propagation path. The crack is assumed to propagate from the top to the bottom of the image.

5. Conclusions

In this study, the mechanical properties of dual-phase (DP) structures with different ferrite grain sizes were investigated, with a particular focus on understanding the mechanisms behind ductility enhancement through grain refinement. Local deformation behavior and micro-void formation/growth were characterized using digital image correlation (DIC) strain analysis and detailed examination of deformation microstructures. The main findings of this study are summarized as follows.

(1) Two types of DP microstructures with ferrite grain sizes of 28.9 μm (coarse-grained) and 11.8 μm (fine-grained) were successfully obtained through heat treatments at 950 °C and 830 °C, respectively, each for 3h followed by furnace cooling, and subsequently heat-treated at 750 °C for 2h followed by water quenching. Apart from the distinct difference in ferrite grain size, both DP specimens exhibited similar martensite volume fractions (~35 %) and phase distributions characterized by chain-like martensite surrounding ferrite grains.

(2) The fine-grained DP specimen exhibited simultaneous improvements in strength and ductility, particularly in post-uniform elongation, as demonstrated by tensile testing. Micro-DIC (μ-DIC) strain analysis revealed that this enhancement was associated with more homogeneous deformation, driven by a greater contribution of martensite to plastic deformation. In contrast, the coarse-grained DP specimen showed pronounced strain localization within the ferrite phase. Regarding strain propagation, thin martensite segments in the coarse-grained DP specimen were ineffective at hindering strain propagation, while large, bulky martensite effectively blocked strain propagation, thereby localizing deformation in the adjacent ferrite grains.

(3) In the post-uniform elongation regime, numerous micro-voids were observed in the necked region of the fine-grained DP specimen; however, most remained small, showing limited void growth. In contrast, the coarse-grained DP specimen exhibited fewer micro-voids, but some of them underwent significant growth. This contrast suggests that the fine-grained DP structure offers greater resistance to void growth, contributing to improved ductility.

(4) In both DP specimens, the propagation paths of micro-voids and the main crack exhibited similar characteristics, preferentially penetrating thin martensite segments while detouring around large martensite regions. These features were predominantly observed in areas with high strain gradients, as revealed by detailed DIC-strain analysis. This finding suggests that strain gradients are a key factor promoting micro-void evolution. Accordingly, the coarse-grained DP specimen, which exhibited more pronounced strain gradients, may have a higher propensity for micro-void growth and subsequent damage accumulation.

(5) The present study suggests that micro-void evolution is influenced by local strain distributions, which may in turn affect the global mechanical properties—particularly the ductility—of the DP structure. The relatively homogeneous deformation observed in the fine-grained DP specimen appears to be associated with suppressed void growth; however, this interpretation requires further validation through more extensive microstructural observation and quantitative analysis.

CRediT authorship contribution statement

Myeong-heom Park: Writing – original draft, Writing – review & editing, Visualization, Methodology, Investigation, Formal analysis, Conceptualization. **Yuichi Tagusari:** Investigation, Formal analysis. **Akinobu Shibata:** Resources, Methodology. **Nobuhiro Tsuji:** Writing – review & editing, Validation, Supervision, Funding acquisition.

Data availability

All data are available upon request.

Declaration of competing interest

The authors declare that they have no known competing financial interests or personal relationships that could have appeared to influence the work reported in this paper.

Acknowledgments

This research work was financially supported by the Elements Strategy Initiative for Structural Materials (ESISM; JPMXP0112101000), JST CREST for Nano-Mechanics (JPMJCR1994), and KAKENHI (Grant-in-Aid for Scientific Research from the Japan

Society for the Promotion of Science; JP22K18888, JP23H00234, JP23K20037, JP20K14608 and JP24K07214), all from the Ministry of Education, Culture, Sports, Science and Technology (MEXT), Japan. All the supports are gratefully appreciated.

References

[1] Calcagnotto M, Ponge D, Raabe D. Effect of grain refinement to 1μm on strength and toughness of dual-phase steels. Mater Sci Eng A 2010;527:7832–40. https://doi.org/10.1016/j.msea.2010.08.062.

[2] Park M-h, Shibata A, Tsuji N. Effect of grain size on mechanical properties of dual phase steels composed of ferrite and martensite. In: MRS Adv; 2016. https://doi.org/10.1557/adv.2016.230.

[3] Azuma M, Goutianos S, Hansen N, Winther G, Huang X. Effect of hardness of martensite and ferrite on void formation in dual phase steel. Mater Sci Technol (United Kingdom) 2012;28:1092–100. https://doi.org/10.1179/1743284712Y.0000000006.

[4] Terada D, Ikeda G, Park M-H, Shibata A, Tsuji N. Reason for high strength and good ductility in dual phase steels composed of soft ferrite and hard martensite. IOP Conf Ser Mater Sci Eng 2017. https://doi.org/10.1088/1757-899X/219/1/012008.

[5] Soliman M, Palkowski H. Tensile properties and bake hardening response of dual phase steels with varied martensite volume fraction. Mater Sci Eng A 2020;777:139044. https://doi.org/10.1016/j.msea.2020.139044.

[6] Il Son Y, Lee YK, Park KT, Lee CS, Shin DH. Ultrafine grained ferrite-martensite dual phase steels fabricated via equal channel angular pressing: microstructure and tensile properties. Acta Mater 2005;53:3125–34. https://doi.org/10.1016/j.actamat.2005.02.015.

[7] Tsuji N, Kamikawa N, Ueji R, Takata N, Koyama H, Terada D. Managing both strength and ductility in ultrafine grained steels. ISIJ Int 2008. https://doi.org/10.2355/isijinternational.48.1114.

[8] Park M-h, Shibata A, Harjo S, Tsuji N. Grain refinement of dual phase steel maximizes deformation ability of martensite, leading to simultaneous enhancement of strength and ductility. Acta Mater 2025;292:121061. https://doi.org/10.1016/j.actamat.2025.121061.

[9] Park M-h, Matsubayashi R, Shibata A, Tsuji N. Quantitative characterization of local deformation-fracture behavior in ferrite-martensite dual-phase steels with different martensite distributions. Mater Sci Eng A 2024;918:147445. https://doi.org/10.1016/j.msea.2024.147445.

[10] Park M-h, Fujimura Y, Shibata A, Tsuji N. Materials Science & Engineering A Effect of martensite hardness on mechanical properties and stress/strain-partitioning behavior in ferrite + martensite dual-phase steels. Mater Sci Eng A 2024;916:147301. https://doi.org/10.1016/j.msea.2024.147301.

[11] Zhang J, Sweedy A, Gitzhofer F, Baroud G. A novel method for repeatedly generating speckle patterns used in digital image correlation. Opt Lasers Eng 2018;100:259–66. https://doi.org/10.1016/j.optlaseng.2017.09.012.

[12] Hamada S, Fujisawa T, Koyama M, Koga N, Nakada N, Tsuchiyama T, Ueda M, Noguchi H. Strain mapping with high spatial resolution across a wide observation range by digital image correlation on plastic replicas. Mater Charact 2014;98:140–6. https://doi.org/10.1016/j.matchar.2014.10.010.

[13] Guo X, Li Y, Suo T, Liu H, Zhang C. Dynamic deformation image de-blurring and image processing for digital imaging correlation measurement. Opt Lasers Eng 2017;98:1339–51. https://doi.org/10.1016/j.optlaseng.2017.05.015.

[14] Chen Y, Wei J, Huang H, Jin W, Yu Q. Application of 3D-DIC to characterize the effect of aggregate size and volume on non-uniform shrinkage strain distribution in concrete. Cem Concr Compos 2018;86:178–89. https://doi.org/10.1016/j.cemconcomp.2017.11.005.

[15] Park K, Nishiyama M, Nakada N, Tsuchiyama T, Takaki S. Effect of the martensite distribution on the strain hardening and ductile fracture behaviors in dual-phase steel. Mater Sci Eng A 2014. https://doi.org/10.1016/j.msea.2014.02.058.

[16] Yan D, Tasan CC, Raabe D. High resolution in situ mapping of microstrain and microstructure evolution reveals damage resistance criteria in dual phase steels. Acta Mater 2015;96:399–409. https://doi.org/10.1016/j.actamat.2015.05.038.

[17] Joo SH, Lee JK, Koo JM, Lee S, Suh DW, Kim HS. Method for measuring nanoscale local strain in a dual phase steel using digital image correlation with nanodot patterns. Scr Mater 2013;68:245–8. https://doi.org/10.1016/j.scriptamat.2012.10.025.

[18] Tasan CC, Hoefnagels JPM, Diehl M, Yan D, Roters F, Raabe D. Strain localization and damage in dual phase steels investigated by coupled in-situ deformation experiments and crystal plasticity simulations. Int J Plast 2014;63:198–210. https://doi.org/10.1016/j.ijplas.2014.06.004.

[19] Saeidi N, Ashrafizadeh F, Niroumand B, Forouzan MR, Barlat F. Damage mechanism and modeling of void nucleation process in a ferrite-martensite dual phase steel. Eng Fract Mech 2014;127:97–103. https://doi.org/10.1016/j.engfracmech.2014.05.017.

[20] Samei J, Green DE, Cheng J, de Carvalho Lima MS. Influence of strain path on nucleation and growth of voids in dual phase steel sheets. Mater Des 2016;92:1028–37. https://doi.org/10.1016/j.matdes.2015.12.103.

[21] Kadkhodapour J, Butz A, Ziaei Rad S. Mechanisms of void formation during tensile testing in a commercial, dual-phase steel. Acta Mater 2011;59:2575–88. https://doi.org/10.1016/j.actamat.2010.12.039.

[22] Ramazani A, Schwedt A, Aretz A, Prahl U, Bleck W. Characterization and modelling of failure initiation in DP steel. Comput Mater Sci 2013;75:35–44. https://doi.org/10.1016/j.commatsci.2013.04.001.

[23] Kang J, Ososkov Y, Embury JD, Wilkinson DS. Digital image correlation studies for microscopic strain distribution and damage in dual phase steels. Scr Mater 2007;56:999–1002. https://doi.org/10.1016/j.scriptamat.2007.01.031.

[24] Erdogan M. The effect of new ferrite content on the tensile fracture behaviour of dual phase steels. J Mater Sci 2002;37:3623–30. https://doi.org/10.1023/A:1016548922555.

[25] Mazinani M, Poole WJ. Effect of martensite plasticity on the deformation behavior of a low-carbon dual-phase steel. Metall Mater Trans A Phys Metall Mater Sci 2007;38:328–39. https://doi.org/10.1007/s11661-006-9023-3.

[26] Tasan CC, Diehl M, Yan D, Bechtold M, Roters F, Schemmann L, Zheng C, Peranio N, Ponge D, Koyama M, Tsuzaki K, Raabe D. An overview of dual-phase steels: advances in microstructure-oriented processing and micromechanically guided design. Annu Rev Mater Res 2015;45:391–431. https://doi.org/10.1146/annurev-matsci-070214-021103.

[27] Park M-h, Shibata A, Tsuji N. Challenging ultra grain refinement of ferrite in low-C steel only by heat treatment. Front Mater 2020;7:1–10. https://doi.org/10.3389/fmats.2020.604792.

[28] Park M-h, Shibata A, Tsuji N. Grain refinement of 2Mn-0.1C steel by repetitive heat treatment and recrystallization. IOP Conf Ser Mater Sci Eng 2015. https://doi.org/10.1088/1757-899X/89/1/012041.

[29] Considère A. Ann Ponts Chaussees 1885;9:574–775.

[30] Briffod F, Shiraiwa T, Enoki M. Micromechanical investigation of the effect of the crystal orientation on the local deformation path and ductile void nucleation in dual-phase steels. Mater Sci Eng A 2021;826:141933. https://doi.org/10.1016/j.msea.2021.141933.

[31] Gu GH, Kwon J, Moon J, Kwon H, Lee J, Kim Y, Kim ES, Seo MH, Hwang H, Kim HS. Determination of damage model parameters using nano- and bulk-scale digital image correlation and the finite element method. J Mater Res Technol 2022;17:392–403. https://doi.org/10.1016/j.jmrt.2022.01.012.

[32] Walpole LJ. The determination of the elastic field of an ellipsoidal inclusion in an anisotronic medium. Math Proc Cambridge Philos Soc 1977;81:283–9. https://doi.org/10.1017/S0305004100053366.

[33] Azuma M. Structural control of void formation in dual phase steels. DTU wind energy. DTU Wind Energy; 2013. PhD No. 0015.

[34] Kim JH, Lee MG, Kim D, Matlock DK, Wagoner RH. Hole-expansion formability of dual-phase steels using representative volume element approach with boundary-smoothing technique. Mater Sci Eng A 2010;527:7353–63. https://doi.org/10.1016/j.msea.2010.07.099.

[35] Hosseini-Toudeshky H, Anbarlooie B, Kadkhodapour J, Shadalooyi G. Microstructural deformation pattern and mechanical behavior analyses of DP600 dual phase steel. Mater Sci Eng A 2014;600:108–21. https://doi.org/10.1016/j.msea.2014.02.016.

[36] Han Q, Asgari A, Hodgson PD, Stanford N. Strain partitioning in dual-phase steels containing tempered martensite. Mater Sci Eng A 2014;611:90–9. https://doi.org/10.1016/j.msea.2014.05.078.

[37] Basu S, Jaya BN, Seekala H, Phani PS, Patra A, Ganguly S, Dutta M, Samajdar I. Correlative characterization and plasticity modeling of microscopic strain localizations in a dual phase steel. Mater Charact 2023;197:112704. https://doi.org/10.1016/j.matchar.2023.112704.

[38] Britton TB, Liang H, Dunne FPE, Wilkinson AJ. The effect of crystal orientation on the indentation response of commercially pure titanium: experiments and simulations. Proc R Soc A Math Phys Eng Sci 2010;466:695–719. https://doi.org/10.1098/rspa.2009.0455.

[39] Ojima M, Adachi Y, Suzuki S, Tomota Y. Stress partitioning behavior in an fcc alloy evaluated by the in situ/ex situ EBSD-Wilkinson method. Acta Mater 2011;59:4177–85. https://doi.org/10.1016/j.actamat.2011.03.042.

[40] Paul SK. Real microstructure based micromechanical model to simulate microstructural level deformation behavior and failure initiation in DP 590 steel. Mater Des 2013;44:397–406. https://doi.org/10.1016/j.matdes.2012.08.023.

[41] Dhole A, Patra A, Gupta RK, Gokhale A, Samajdar I. Surface hardening through oxygen diffusion in niobium: the defining role of stress inhomogeneity in tensile embrittlement. Mater Sci Eng A 2023;870:144883. https://doi.org/10.1016/j.msea.2023.144883.

[42] Yin W, Briffod F, Hu H, Yamazaki K, Shiraiwa T, Enoki M. Role of prior austenite grain boundary and retained austenite in strain localization of medium-carbon high-strength steels. Acta Mater 2024;281. https://doi.org/10.1016/j.actamat.2024.120422.

[43] Paul SK, Stanford N, Hilditch T. Effect of martensite morphology on low cycle fatigue behaviour of dual phase steels: experimental and microstructural investigation. Mater Sci Eng A 2015;644:53–60. https://doi.org/10.1016/j.msea.2015.07.044.

[44] Paul SK, Stanford N, Hilditch T. Effect of martensite volume fraction on low cycle fatigue behaviour of dual phase steels: experimental and microstructural investigation. Mater Sci Eng A 2015;638:296–304. https://doi.org/10.1016/j.msea.2015.04.059.